SIAM J. APPL. MATH.
Vol. 60, No. 6, pp. 2009–2028

DYNAMICS OF NEURONAL POPULATIONS: THE EQUILIBRIUM SOLUTION*

L. SIROVICH†‡, A. OMURTAG†, AND B. W. KNIGHT†‡

Abstract. The behavior of an aggregate of neurons is followed by means of a population equation which describes the probability density of neurons as a function of membrane potential. The model is based on integrate-and-fire membrane dynamics and a synaptic dynamics which produce a fixed potential jump in response to stimulation. In spite of the simplicity of the model, it gives rise to a rich variety of behaviors. Here only the equilibrium problem is considered in detail. Expressions for the population density and firing rate over a range of parameters are obtained and compared with like forms obtained from the diffusion approximation. The introduction of the jump response to stimulation produces a delay term in the equations, which in turn leads to analytical challenges. A variety of asymptotic techniques render the problem solvable. The asymptotic results show excellent agreement with direct numerical simulations.

Key words. neuronal models, kinetic equations, equilibria

AMS subject classifications. 92C05, 92C20, 92B20

PII. S0036139998344921

1. Introduction.

Quantitative modeling of nervous tissue such as that found in the cortex involves both complexity and detail. As an indication of this we note that distinct cortical areas contain $O\left(10^8\right)$ neurons and a cortical neuron can interact with as many as $O\left(10^5\right)$ other neurons, [2]. Further, the neuronal and synaptic dynamics are themselves complex; the range of time scales experienced in laboratory experiments on cortex vary from fractions of a millisecond to tens of seconds. Such ingredients vastly increase the difficulty in simulating such a system. Nevertheless, with precise information on individual neurons, the blueprint of connectivity, and limitless computational resources, one might, in principle, obtain dynamical predictions of entire systems. Large scale direct simulations with modest goals have been investigated ([22], [4], [17]; see also the articles in [10], [12]).

A philosophically different approach to the simulation of aggregates of neurons is to address the statistical dynamical behavior of populations directly. This approach is based on the observation that the cortex may be regarded as a collection of relatively homogeneous patches, each composed of about 10^4 neurons and with only a small number of specific neuronal types within any particular patch. That perspective is adopted in this investigation. This is a newer and less well-studied approach. An early contribution with this modern viewpoint is the thesis of Johannesma [6]. Another early effort was carried out by Knight [7] in connection with experimental research on the limulus retina. More recently a related population approach has been taken up in several studies [1], [5], [9], [3]. The presentation that follows is based on the formulation of [9] and two more recent expositions [8], [14].

*Received by the editors September 21, 1998; accepted for publication (in revised form) May 28, 1999; published electronically June 3, 2000. This work was supported by NIH/NIMH MH50166, NIH/NEI EY11276, ONR N00014-96-1-0492, and ONR N0014–96-1-5005. This and related literature can be found at http://camelot.mssm.edu/.

http://www.siam.org/journals/siap/60-6/34492.html

†Laboratory of Applied Mathematics, Mount Sinai School of Medicine, One Gustave L. Levy Place, New York, NY 10029-6574 (chico@camelot.mssm.edu).

‡Rockefeller University, 1230 York Avenue, New York, NY 10021 (knight@rockvax.rockefeller.edu).

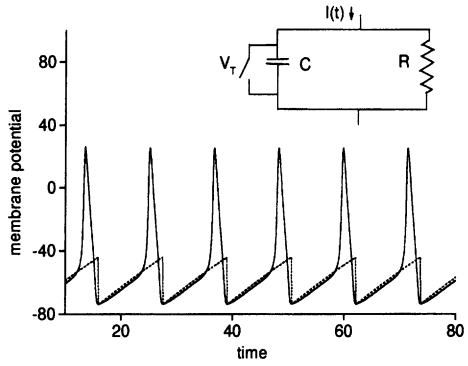

FIG. 1. *Hodgkin–Huxley neuron stimulated by a constant current* ($10\mu A$) *is shown together with the membrane potential of the integrate-and-fire neuron. To obtain the latter, the value* $\gamma = 20$ ($\sec^{-1}$) *is used in* (3). *All subsequent calculations in this paper use the same value for* γ. *The equivalent electrical circuit represented by* (1) *appears as an inset in this figure.*

It is our intention here to examine the structure of a minimal, but relatively useful, population model. Membrane dynamics will be modeled by the integrate-and-fire equation, and synaptic dynamics (the dynamics of input) by a fixed potential jump response to each synaptic event. In the spirit of simplicity only excitatory interactions (positive feedback) will be discussed. The chief goal is to develop an understanding of the structure of the population equation and simultaneously to develop a set of analytical tools which can be extended to populations of more detailed neurons and more complex networks. Some discussion of such extensions appears in the concluding section.

2. Formulation. We consider a *patch* of nervous tissue composed of like neurons. A single neuron generates a train of action potentials, as shown in Figure 1. A familiar feature of neuronal dynamics is that when the membrane potential, V, reaches a threshold, it produces a spike of relatively short duration. This process may be approximated by the saw-tooth-like curve of Figure 1, which in turn can be modeled by the simple circuit equation

$$I = C\frac{dV}{dt} + \frac{1}{R}V, \tag{1}$$

as indicated in the figure. Under this model the potential builds up until the threshold V_T is reached, at which point the potential is reset to the resting state, which may be chosen as zero. This is known as the (forgetful or "leaky") integrate-and-fire model [19].

This model has played an important role in many discussions of collective oscillations of coupled oscillators [15], [13], [20], [1]. If we take

$$\gamma = 1/RC, s = I/CV_T, \quad v = V/V_T, \tag{2}$$

then

$$\frac{dv}{dt} = -\gamma v + s; \ 0 \le v \le 1 \tag{3}$$

is the normalized form of the dynamics. Both γ and s have the units of inverse time, although the latter is more properly said to be a current. Note that the model is actually nonlinear as a result of the presence of a threshold.

The input signal is neuronal and is specified as a firing rate: it has the units of inverse time. Synaptic arrivals at a neuronal membrane produce conductance changes, which in turn produce a change in the membrane voltage. If the relatively short time scale of synaptic dynamics is ignored, the situation can be modeled by membrane voltage jumps which we take as size, h. Their arrival times are denoted by $\{t_k\}$ and individual neurons follow the equation

$$\frac{dv}{dt} = -\gamma v + h \sum_k \delta(t - t_k), \tag{4}$$

where v is reset to zero whenever it exceeds unity.

Direct simulations. Results of the analysis to be presented will be compared with the direct simulation of a large population of neurons, each of which follows the dynamics of (4). In such simulations each neuron receives its own Poisson distribution of arrival times. The only additional ingredient needed to carry out such a simulation is the *blueprint* of connections. If the neurons are indexed, this is conveniently envisioned as a matrix of connectivities. For simplicity only excitatory connections are considered. To avoid runaway that accompanies such positive feedback the network is sparsely connected. Equivalently, one may consider the network to be coupled in an all-to-all fashion but with a high synaptic failure rate; see Abeles [2] for a discussion of this point. In any case the connectivity matrix is thought of as drawn from an ensemble of random matrices with a specified average number of connections, which we denote by G, the gain. A (perhaps subtle) point is that the connectivity matrix should be drawn anew from the ensemble after each neuronal firing. Otherwise, if the connectivity is held fixed, a neuron takes on an explicit identity and we no longer have a population of like neurons. These and related considerations are more fully addressed in [14].

Population model. Since the population of neurons is regarded as homogeneous, it is natural to consider the probability of finding a neuron in the state v and this will be denoted by $\rho(v,t)$. Thus $\rho(v,t)\,dv$ denotes the fraction of neurons in the range $(v, v+dv)$ at time t. We denote the flux of probability, within the interval $0 \le v \le 1$, by J, which from continuity is related to the density ρ through

$$\frac{\partial \rho}{\partial t} = -\frac{\partial J}{\partial v}. \tag{5}$$

Since each synaptic arrival induces a voltage jump of h, the arrival rate is $s(t)/h$. From this it follows that

$$J(v,t) = -\gamma v \rho + \frac{s}{h} \int_{v-h}^{v} \rho(v')\,dv', \tag{6}$$

so that

$$\frac{\partial}{\partial t}\rho = \frac{\partial}{\partial v}(\gamma v \rho) + \frac{s}{h}(\rho(v-h) - \rho(v)) = L\rho;\ 0 \le v \le 1. \tag{7}$$

This equation was also obtained in the study of neuronal variability by Wilbur and Rinzel [21] and somewhat earlier by Stein [18]. A formal derivation of (7) based on the concept of an ensemble average over direct simulations, as discussed above, is presented in [14]. From this it follows that, in the limit of a large number of neurons, the solution of (7) and the direct simulation should agree. This is extensively discussed in [14], and illustrations of this will be given below.

The per-neuron firing rate, $r(t)$, of the population is a variable of interest. For our simplified model this is manifestly given by

$$r(t) = J(v = 1, t). \tag{8}$$

The ensemble average, over all synaptic arrivals, produces the synaptic arrival rate denoted by σ, so that the *current*, s, in (6) is given by

$$s = \sigma h. \tag{9}$$

Sources of synaptic arrivals are twofold, external and internal feedback. The former we denote by $\sigma^0(t)$, while the latter is given by the product $Gr(t)$, where G is the earlier defined gain (average number of connections per neuron) and $r(t)$, (8), the population firing rate per neuron. Thus

$$\sigma = \sigma^0(t) + Gr(t), \tag{10}$$

which indicates another nonlinearity of the formulation. Equation (10) implies that each neuron of the population *feels* the population firing rate, $r(t)$. This might be regarded as a *dynamic mean field* approximation, [5].

Boundary conditions. The flux of probability leaving the unit interval must equal the flux entering, thus the jump in J across the interval, denoted by $[J(\rho)]$, must vanish:

$$[J(\rho)] = J(\rho)|_{v=1} - J(\rho)|_{v=0} = 0. \tag{11}$$

This guarantees that

$$\frac{\partial}{\partial t}\int_0^1 \rho(v)\, dv = 0 \tag{12}$$

and, in keeping with the interpretation of ρ as a probability, the constant of integration will be taken as unity:

$$\int_0^1 \rho(v)\, dv = 1. \tag{13}$$

Although only one space derivative in v appears in (7), two boundary conditions are required. This is a consequence of the *delay* term in (7). The second boundary condition is that

$$\rho(1) = 0. \tag{14}$$

To see this observe that (6) contains a *backward* moving flux, $-\gamma v\rho$, as well as the remaining forward-jumping portion which gives a forward convection. Since only the latter term can contribute at $v = 1$, we must have (14).

The eigenfunction problem. An eigenfunction analysis of the operator L in (7),

$$\left.\begin{array}{rcl} L\phi & = & -\lambda\phi; \\ \phi(1) & = & 0 = [J(\phi)] \end{array}\right\}, \tag{15}$$

may be regarded as a natural method for unraveling the structure of the dynamical problem. While we do not pursue this here we observe that $\lambda = 0$ in (15) furnishes the equilibrium solution. This is the focus of our analysis.

The equilibrium problem. It follows from (6) that the equilibrium solution in response to constant current, s_0, satisfies

$$-\gamma v\rho + \frac{s_0}{h}\int_{v-h}^{v} \rho(v')\,dv' = J_0, \tag{16}$$

where the flux, J_0, is a constant. In particular the constant firing rate is

$$r_0 = \frac{s_0}{h}\int_{1-h}^{1} \rho(v')\,dv = \sigma_0 \int_{1-h}^{1} \rho(v')\,dv' \,(= J_0) \tag{17}$$

since $\rho(1) = 0$, from (14). Thus from (10)

$$r_0 = \left(\sigma^0 + Gr_0\right)\int_{1-h}^{1} \rho(v')\,dv', \tag{18}$$

so that

$$r_0 = \frac{\sigma^0 \int_{1-h}^{1} \rho(v')\,dv'}{1 - G\int_{1-h}^{1} \rho(v')\,dv'}. \tag{19}$$

We first observe that by fixing σ_0 the problem of solving (7) becomes linear, and second that from (18) this generates a locus of solutions with varying input σ^0 and gain G. The possible divergence of (19) is closely related to the issue of stability which is considered elsewhere [16].

It is convenient to consider instead of ρ

$$\phi(v) = \frac{s}{J_0}\rho, \tag{20}$$

which may be regarded as the eigenfunction of L corresponding to $\lambda = 0$. Then instead of (16) we consider

$$-\frac{\gamma}{s}v\phi + \frac{1}{h}\int_{v-h}^{v} \phi(v')\,dv' = 1. \tag{21}$$

If (20) is introduced into (13), once (21) is solved for $\phi(v)$, the firing rate is determined by

$$J_0 = s\left[\int_0^1 \phi(v)\,dv\right]^{-1}. \tag{22}$$

The remainder of the paper deals with the analytical solution of (21) and how this compares with direct simulations of a population which contains a large number of integrators which follow (4). In the direct simulation the population of neurons might be stimulated by a constant input and after an initial transient equilibrium sets in.

The elementary form of the linear equation (21) belies the complexity to which it gives rise. In fact as summarized in section 9 there are four well-defined regions, each of which requires different mathematical tools. A naive approach takes advantage of the smallness of h (based on physiological considerations we fix the normalized value of h to be .03). As we see next this leads to diffusion theory. This both is interesting in its own right and sets the stage for later deliberations.

3. Diffusion approximation. It is useful to consider (21) under the formal limit $h \downarrow 0$. We can expect this to be nonuniform but valid for some still to be determined region $0 < v < 1$. Under this limit (21) yields

$$-\frac{\gamma}{s}v\phi + \phi = 1, \tag{23}$$

from which it follows that

$$\phi = \frac{1}{1 - \gamma v/s}. \tag{24}$$

In order for the denominator to remain positive in the interval we must have $s - \gamma > 0$. If (24) is substituted into (22) we obtain

$$J_0 = \frac{-\gamma}{\ln(1 - \gamma/s)} \tag{25}$$

for the population firing rate. Note, that when $s >> \gamma$, then $J_0 \approx s$, which says that the firing rate tracks the current, as one might expect. In fact (25) is the firing rate of a single integrator in response to a constant current. Through one more order in γ/s, we calculate

$$J_0/\gamma \approx (s/\gamma) - \frac{1}{2} \tag{26}$$

for $s >> \gamma$, which extrapolates to 0 at $s/\gamma = \frac{1}{2}$ while the exact result (24) vanishes (gives zero firing rate) at $s/\gamma = 1$.

In the terminology of matched asymptotic expansions the integrate-and-fire solution, (25), is the *outer solution.* It fails to meet the boundary conditions at both endpoints of the interval. Also when $s/\gamma < 1$, since (24) is divergent at $v = s/\gamma$, an *internal boundary layer* appears to be necessary. Both considerations would appear to be met by proceeding to the next term of the Taylor expansion in h of the integral in (21):

$$\left(1 - \frac{\gamma}{s}v\right)\phi - \frac{h}{2}\frac{\partial\phi}{\partial v} = 1. \tag{27}$$

It is worth observing that when this is done in the framework of (7) we obtain the diffusion equation

$$\frac{\partial}{\partial t}\phi = \frac{\partial}{\partial v}(\gamma v - s)\phi + \frac{sh}{2}\frac{\partial^2\phi}{\partial v^2}. \tag{28}$$

Under the boundary conditions (11) and (14), integration of (27) yields

$$\phi = \frac{2}{h}\exp\left[-\left(\frac{h\gamma}{s}\left(\frac{v}{h}\right)^2 - 2\frac{v}{h}\right)\right]\int_v^1 \exp\left[\left(\frac{h\gamma}{s}\left(\frac{v'}{h}\right)^2 - 2\frac{v'}{h}\right)\right]dv'. \tag{29}$$

We see in (29) that the normalized potential v is scaled with h. The exponent also contains the ratio of the two rates present in (7),

$$\frac{\sigma}{\gamma} = \frac{s}{\gamma h} = \theta. \tag{30}$$

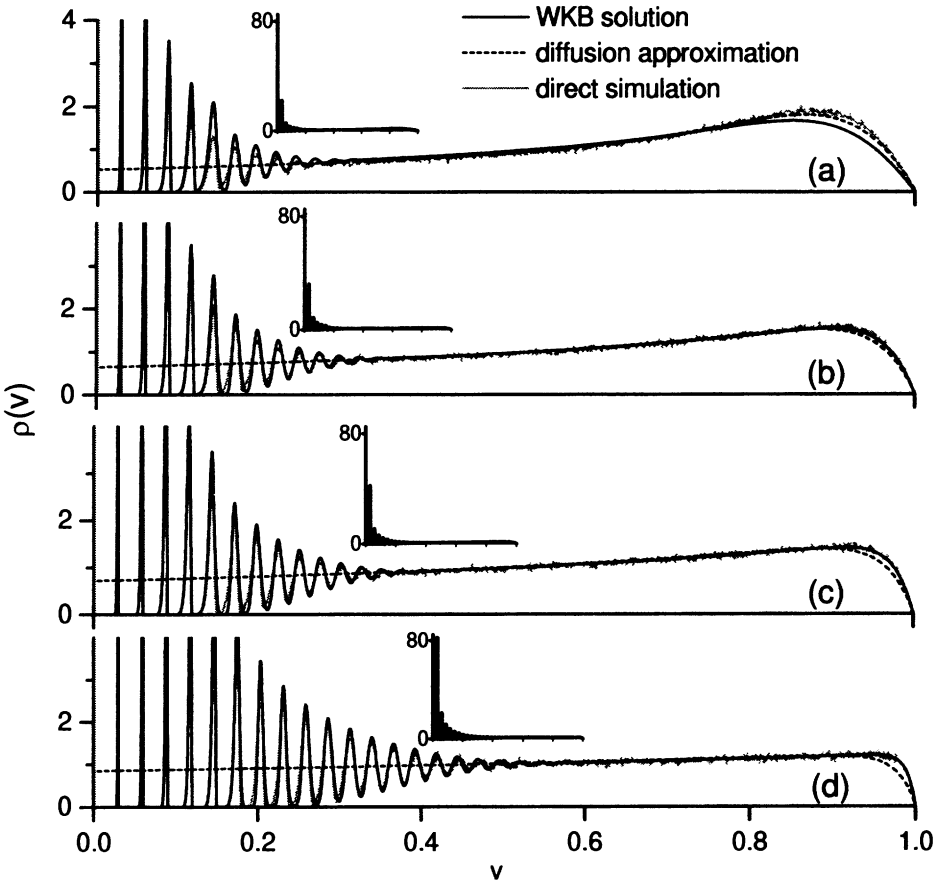

FIG. 2. *The normalized probability density at equilibrium with* (a) $\theta = 40$, (b) $\theta = 50$, (c) $\theta = 60$, *and* (d) $\theta = 100$. *The gray jagged curve represents the density of a population of* 10^4 *noncommunicating integrate-and-fire neurons computed by direct simulation and averaged over a period of three seconds after reaching equilibrium* [14]. *The dashed curve is the density obtained at the diffusion limit. The combined inner, WKB, and outer solutions are shown as the solid curves. For the purpose of illustration the peaks have been clipped. Insets in each case show the full range of variation. In these and all subsequent calculations* $h = 0.03$.

This dimensionless ratio is a large parameter of the problem. In typical situations, it lies in the range, $40 < \theta < 100$.

If (29) is substituted into (22) this yields J_0/γ as a function of s/γ:

$$\left(\frac{J_0}{\gamma}\right)^{-1} = -\frac{2}{h}\int_0^1 dv \ln v \left\{\left(\frac{\gamma}{s}(1-v)-1\right)\exp\left[-\left(\frac{\gamma v^2}{hs}+\frac{2v}{h}\left(\frac{\gamma}{s}-1\right)\right)\right]\right.$$
$$\left. -\left(\frac{v\gamma}{s}-1\right)\exp\left[\left(\frac{\gamma v^2}{hs}-\frac{2v}{h}\right)\right]\right\}. \tag{31}$$

The equilibrium solution (29) is plotted in Figure 2 for several values of θ and the corresponding population firing frequency (31) is plotted in Figure 3.

The exact equation governing equilibrium is

$$\frac{1}{\theta}\frac{d}{dv}(v\phi) = \phi(v) - \phi(v-h), \tag{32}$$

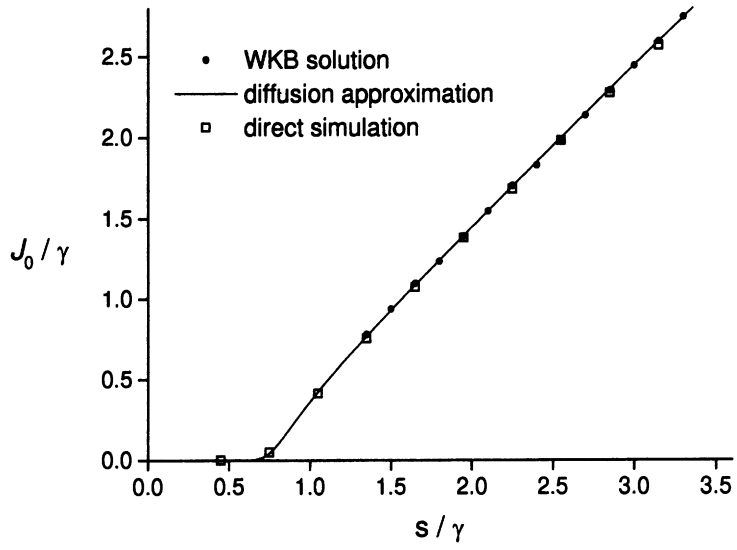

FIG. 3. *The equilibrium firing rate normalized with respect to γ plotted as a function of s/γ. The continuous curve is calculated using the diffusion approximation. The squares are obtained from direct simulations as described in Figure 2. The firing rates given by the WKB solution are shown by the filled circle symbols.*

and from (21) a first integral is

$$\theta \int_{v-h}^{v} \phi(v')\, dv' - v\phi(v) = \frac{s}{\gamma}. \tag{33}$$

Although (32) is only first order as a differential equation, the presence of the delay term suggests that some complexity can be expected. The well-known equation of Mackey and Glass [11] provides an example of the complexity which can appear as a result of a delay term.

Within the framework of the posed problem, we may take

$$\phi(v) \equiv 0, \quad v \notin [0,1]. \tag{34}$$

Thus when v is less than h, the delayed second term on the right in (32) is zero. This special case is easily integrated and the solution in this range is

$$\phi(v) = h\delta(v) + \phi(h^-)\left(\frac{v}{h}\right)^{\theta-1}; \quad 0 \le v \le h. \tag{35}$$

The appearance of the delta function term, which clearly satisfies (33), is due to the accumulation of members of the population at the origin from the flux at $v = 1$. If the solution (35) is substituted into (32) it permits us to exactly calculate ϕ in the second interval, $[h, 2h]$, in terms of an integral. On proceeding in this way we may recursively determine ϕ throughout the interval, with a finite number of integrations.

In preparation for this procedure each subinterval is normalized to unit length, and we write

$$\Phi_n(z) = \phi(nh + zh); \quad 0 \le z \le 1. \tag{36}$$

Equation (32) can then be put in the form

$$\frac{d}{dz}\left[(n+z)^{\theta-1}\,\Phi_n\right] = -\theta\,(n+z)^{-\theta}\,\Phi_{n-1}(z)\,, \tag{37}$$

which integrates to give

$$\Phi_n(z) = \left(1+\frac{z}{n}\right)^{\theta-1}\Phi_n^0 - \theta\,(n+z)^{\theta-1}\int_0^z \frac{\Phi_{n-1}(z')\,dz'}{(n+z')^{\theta}}. \tag{38}$$

At any point of continuity we write

$$\Phi_n^0 = \Phi_n(0) = \Phi_{n-1}(1)\,. \tag{39}$$

From (35) we see that in the first interval

$$\Phi_0(z) = \delta(z) + \phi^- z^{\theta-1}, \tag{40}$$

where $\phi^- = \phi(h^-)$. As a result of the presence of the delta function at the origin $\phi(v)$ is discontinuous at $v = h$. ϕ therefore has a discontinuous first derivative at $v = 2h$, a discontinuous second derivative at $v = 3h$, and so forth. Hence (39) holds for $n > 1$.

In the case $n = 1$ we may substitute (40) into (38) to obtain

$$\Phi_1(z) = \left(\phi^- - \theta\right)(1+z)^{\theta-1} - \theta\,(1+z)^{\theta-1}\int_0^z \frac{s^{\theta-1}ds}{(1+s)^{\theta}}\phi^-. \tag{41}$$

Clearly

$$\phi^+ = \phi^- - \theta \tag{42}$$

is the value of ϕ at $v = h$ as we approach this point from the right. Recursive substitution into (38) now provides the solution throughout the interval $0 \le v \le 1$. Note that at this stage (42) supplies the jump in $\phi(v)$ at $v = h$, but neither ϕ^+ nor ϕ^- are known. Only after the boundary conditions are imposed can we expect to determine these.

A practical difficulty of this procedure is now apparent from (41). At the endpoint of our small interval where $z \to 1$, the constant $\phi^+ (= \phi^- - \theta, (42))$ has a coefficient $2^{\theta-1}$, which is $O\left(10^{30}\right)$ if $\theta = 100$. Since we anticipate that $\phi = O(1)$, ϕ^+ must be correspondingly small. The situation of extreme smallness and largeness places a burden on machine calculations since high precision is needed. This leads to numerical difficulties which may be avoided by the use of asymptotic approximations.

4. Asymptotic analysis of the inner region. For many reasons it is desirable to have an analytical form for the solution. In this spirit we introduce an asymptotic analysis on the basis of $\theta \uparrow \infty$. The density in successive intervals is given by (38). The collection of early intervals will be referred to loosely as the *inner region.*

The integral in (41) lends itself to asymptotic evaluation for $\theta \uparrow \infty$. From (A5) in the appendix we obtain

$$\int_0^z \frac{s^{\theta-1}ds}{(1+s)^{\theta-1}} \sim \frac{z^{\theta-1}}{(\theta-1)\,(1+z)^{\theta-1}}, \tag{43}$$

which substituted into (41) yields

$$\Phi_1(z) \sim (1+z)^{\theta-1}\Phi_1^0 - \frac{\theta}{\theta-1}z^\theta\phi^-, \tag{44}$$

whence

$$\Phi_2^0 = \Phi_2(0) = \Phi_1(1) \sim 2^{\theta-1}\Phi_1^0 - \frac{\theta}{\theta-1}\phi^-. \tag{45}$$

Thus (44) may be rewritten as

$$\Phi_1(z) \sim \left(\frac{1+z}{2}\right)^{\theta-1}\Phi_2^0 + \left[\left(\frac{1+z}{2}\right)^{\theta-1} - z^\theta\right]\frac{\theta}{\theta-1}\phi^-. \tag{46}$$

To obtain $\Phi_2(z)$ we substitute (44) under the integral of (38) and again asymptotically evaluate the integral (see appendix). In this way we may recursively obtain $\Phi_n(z)$. The result is

$$\Phi_n(z) \sim \sum_{k=0}^{n-1}\left(-\frac{\theta}{\theta-1}\right)^k \frac{(n+z-k)^{\theta-1+k}}{(n-k)^{\theta-1}}\frac{\Phi_{n-k}^0}{k!} + \left(\frac{-\theta}{\theta-1}\right)^n z^{\theta-1+n}\frac{\phi^-}{n!}, \tag{47}$$

for $n = 1, 2, \ldots$, with $\Phi_1^0 = \phi^+$. As pointed out in the appendix the above forms are valid when $n << \sqrt{\theta}$.

As Figure 2 indicates the solution exhibits several ranges of behavior. The inner region, just discussed, gives way to a smoother intermediate zone which connects to the outer solution, (19), which finally connects to an outer boundary layer that takes ϕ to its zero value at the right endpoint, $v = 1$. We will deal with this in generality in the next section. For the moment it is useful to see how these regions are described under the diffusion approximation. Equation (29) may be made more transparent under the $h \downarrow 0$ asymptotics. In this case, for $s \geq \gamma$ (see (24)), the integrand has a sharp maximum at the left endpoint. Because of this one easily finds

$$\phi \sim \frac{1}{1-\gamma v/s}\left(1 - \exp\left[-2\left(1-\frac{\gamma v}{s}\right)\left(\frac{1-v}{h}\right)\right]\right), \tag{48}$$

which clearly exhibits a narrow, $O(h)$ boundary layer at the right endpoint, $v = 1$, which (as will be seen) can be incorrect in detail. This form is clearly incorrect for the inner region, but it does show transition to the outer solution (24).

5. WKB asymptotics. The diffusion limit which appears in (21) is based on the expansion

$$\phi(v-h) - \phi(v) \sim \sum_{n=1}\frac{1}{n!}\left(-h\frac{\partial}{\partial v}\right)^n \phi(v), \tag{49}$$

taken through two orders. However, as is clear from (48) this leads to a solution for which $\left(h\frac{\partial}{\partial v}\right)^n = O(1)$ when $v \approx 1$, and thus the approximation is cast into doubt. Moreover, as is seen in Figure 2 there is a wide region of the interval, beyond the inner zone where the local scale size is $O(h)$. To capture such *fast* scales we first expand the interval under the transformation,

$$\xi = \frac{v}{h} \tag{50}$$

so that

$$\Phi(\xi) = \phi(\xi h), \tag{51}$$

and thus (32) becomes

$$\frac{1}{\theta}\frac{d}{d\xi}(\xi\Phi) = \Phi(\xi) - \Phi(\xi - 1), \quad 0 \le \xi \le \frac{1}{h}. \tag{52}$$

ξ, which is v rescaled, ranges from 0 to $1/h$. Note that from (36)

$$\Phi(n + z) = \Phi_n(z). \tag{53}$$

WKB analysis. The WKB method offers us a framework for treating the two-scale effects observed in Figure 2. To carry out this procedure we seek solutions of (52) in the form

$$\varphi(\xi) = \exp\left[\theta \int_{\xi_*/\theta}^{\xi/\theta} \alpha(t;\theta)\, dt\right]. \tag{54}$$

The integrand α plays the role of a slowly varying (complex) *wavenumber.* The ratio

$$\xi/\theta = \tilde{\xi} \tag{55}$$

is slow and the lower endpoint $\tilde{\xi}^* = \xi^*/\theta$ is chosen to be a convenient reference point. The dependent variable to be found is supposed to have the expansion

$$\alpha(t;\theta) = \alpha^0(t) + \frac{1}{\theta}\alpha^1(t) + \frac{1}{\theta^2}\alpha^2(t) + \cdots. \tag{56}$$

The solution $\Phi(\xi)$ to (52) will be seen to be a superposition of solutions of the form (54). If (54) is substituted into (52) we obtain

$$\frac{1}{\theta} + \tilde{\xi}\alpha\left(\tilde{\xi};\theta\right) = 1 - \frac{\varphi(\xi - 1)}{\varphi(\xi)}. \tag{57}$$

From the supposed solution, (54), the ratio on the right is given by

(58)

$$\frac{\varphi(\xi - 1)}{\varphi(\xi)} = \exp\left[-\theta \int_{(\xi-1)/\theta}^{\xi/\theta} \alpha(t;\theta)\, dt,\right] = \exp\left[-\alpha\left(\tilde{\xi};\theta\right) + \frac{1}{2\theta}\alpha'\left(\tilde{\xi}\right) + 0\left(\frac{1}{\theta^2}\right)\right],$$

where the integrand has been developed in a Taylor expansion about the upper endpoint, $\tilde{\xi} = \xi/\theta$, to get the second form. If this is substituted into (57) we obtain

$$\frac{1}{\theta} + \tilde{\xi}\alpha(t;\theta) = 1 - \left[1 + \frac{\alpha'(\tilde{\xi};\theta)}{2\theta} + O\left(\frac{1}{\theta^2}\right)\right]\exp\left[-\alpha\left(\tilde{\xi};\theta\right)\right]. \tag{59}$$

Next the development of $\alpha(\tilde{\xi};\theta)$, (56), is substituted into (59). To lowest order we obtain the dispersion relation,

$$\tilde{\xi}\alpha^0 = 1 - e^{-\alpha^0}, \tag{60}$$

and at the next order we find

$$1+\widetilde{\xi}\alpha^1 = -e^{-\alpha^0}\left(\frac{(\alpha^0)'}{2}-\alpha^1\right). \tag{61}$$

As shown in the appendix there are two real roots to (60), $\alpha_0^0 = 0$ and another which we denote by α_+^0 since it is positive. All other roots occur in complex conjugate pairs α_k and $\overline{\alpha}_k$ and have negative real parts. We denote the corresponding WKB solutions by $\varphi_0, \varphi_+, \varphi_k, \overline{\varphi}_k$. It remains for us to determine the admixture of these WKB solutions needed to solve the problem.

A model problem. For this purpose we return to (52) and consider the equation in the neighborhood of the reference point ξ_*,

$$\frac{\xi_*}{\theta}\frac{d}{d\xi}\Phi(\xi) = \Phi(\xi)-\Phi(\xi-1);\quad \xi_* \le \xi < \infty. \tag{62}$$

Equation (62) is translationally invariant and may be solved by transform methods. For ξ near ξ_* (62) approximates the solution to the problem. We further specify ξ_* by taking it to be the endpoint of an interval ξ_* and therefore an integer. On applying the Laplace transform to (62) the solution is found to be

$$\Phi(\xi) = \frac{1}{2\pi i}\int_{\uparrow}\frac{e^{\sigma(\xi-\xi_*)}\widetilde{\xi}_*\Phi_k^0 - \Phi^k(\sigma)}{\widetilde{\xi}_*\sigma - 1 + e^{-\sigma}}d\sigma, \tag{63}$$

where $\uparrow$ denotes an appropriate Bromwich path. As a result of the delay term in (62), $\Phi(\xi)$ for $\xi_* - 1 < \xi < \xi_*$ also figures in the solution which accounts for the presence of

$$\Phi^k(\sigma) = \int_0^1 e^{-\tau\sigma}\Phi(k-1+\tau)\,d\tau = \int_0^1 e^{-\tau\sigma}\Phi_{k-1}(\tau)\,d\tau \tag{64}$$

in the solution (63).

The roots of the *dispersion relation*, the denominator in (63),

$$\widetilde{\xi}_*\sigma - 1 + e^{-\sigma} = 0 \tag{65}$$

are derived in the appendix. In the present case, $0 < \widetilde{\xi}_* << 1$. In this instance $\sigma_0 = 0$ and $\sigma_+ \sim 1/\widetilde{\xi}_*$ are roots, in addition to which there are infinitely many conjugate pairs $\sigma_k, \overline{\sigma}_k$, all of which have negative real parts. In residue form we may write the solution (63) as

$$\Phi(\xi) = e^{\sigma_+(\xi-\xi_*)}C_+ + C_0 e^{\sigma_0} + \sum_k\left(e^{\sigma_k(\xi-\xi_*)}C_k + c.c.\right), \tag{66}$$

where the pole-strengths determine

$$C_k = \frac{\Phi_k^0\widetilde{\xi}_* - \Phi^k(\sigma_k)}{\widetilde{\xi}_* - e^{-\sigma_k}} \tag{67}$$

with corresponding definitions for C_+ and C_0.

WKB solution. We now observe that the WKB solution to our problem is given by

$$\Phi(\xi) = \varphi_+ C_+ + \varphi_0 C_0 + \sum_k \left(\varphi_k C_k + \overline{\varphi}_k \overline{C}_k\right), \tag{68}$$

where the indexing of the φs follows that of the αs. Clearly for small ξ each WKB solution φ_k is well approximated by the corresponding exponential which occurs in (66), and thus we recover the appropriate solution in the neighborhood of $\xi = \xi_*$. Beyond the neighborhood of ξ near ξ_*, each of the terms $\varphi_+, \varphi_0, \varphi_k, \overline{\varphi}_k$ is a solution to (52) to any desired order in inverse powers of θ. We further argue that (68) is valid from the inner through the outer region including the right-hand endpoint.

6. Boundary layer. In the neighborhood of the right endpoint $v = 1$, $\xi = 1/h$ (or $\widetilde{\xi} = \gamma/s$), all WKB modes are exponentially small with the exception of φ_0 and φ_+.

Therefore, as we approach the right-hand endpoint, the summation in (68) decays exponentially and we have

$$\Phi(\xi) \sim \varphi_0 C_0 + \varphi_+ C_+. \tag{69}$$

To determine φ_0 we recall that $\alpha_0^0 = 0$ and so observe from (61) that through the first two orders of α_0,

$$\alpha_0(t) = \frac{1}{\theta}\frac{1}{1-t} + O\left(\frac{1}{\theta^2}\right); \tag{70}$$

it therefore follows from (54) that

$$\varphi_0 \sim \frac{1-\widetilde{\xi}_*}{1-\widetilde{\xi}}. \tag{71}$$

For the second term in (69), φ_+, we simply write

$$\varphi_+ \sim e^{\theta \int_{\widetilde{\xi}_*}^{\widetilde{\xi}} \alpha_+(t)dt} \tag{72}$$

and leave open for the moment the number of terms of $\alpha_+(t;\theta)$ which will be used.

The asymptotic form for C_0 is given by (A16) and we find

$$\varphi_0 C_0 \sim \frac{1}{1-\widetilde{\xi}} = \frac{1}{1-\gamma v/s}, \tag{73}$$

which is just the outer integrate-and-fire result, (24).

If this is substituted into (69) and the boundary condition $\Phi(1/h) = 0$ is imposed, we obtain

$$0 = \frac{1}{1-\gamma/s} + C_+ e^{\theta \int_{\widetilde{\xi}_*}^{\gamma/s} \alpha_+(t)dt} \tag{74}$$

since $(h\theta)^{-1} = \gamma/s$. This is solved for C_+ and when the result is introduced into (69) the integral in the exponential of C_+ combines with that in φ_+ and we obtain

$$\Phi(\xi) \sim \frac{1}{1-\xi/\theta}\left[1 - \frac{1-\xi/\theta}{1-\gamma/s}\exp\left(-\theta\int_{\xi/\theta}^{\gamma/s}\alpha_+(t)\,dt\right)\right]. \tag{75}$$

The second term of (75) which is $C_+\varphi_+$, clearly is exponentially small unless $v\,(=\xi/\theta)$ is near γ/s. Thus it describes the right-hand $0\left(\theta^{-1}\right)$boundary layer. In our calculations we have used just two orders in $\alpha_+(t)$.

7. Inner transition. From (74) it is clear that C_+ is exponentially small in θ. As shown in the appendix, (A17), this implies that

$$\Phi_2^0 \approx \frac{\theta^2}{2} e^{-\theta/2}. \tag{76}$$

Therefore with the exception of the neighborhood of the right endpoint the contribution to (68) from $\varphi_+ C_+$ is negligible. Thus the transition from the integrate-and-fire region to the inner region is described by

$$\Phi(\xi) \sim \frac{1}{1-\tilde{\xi}} + \sum_k (\varphi_k C_k + c.c), \tag{77}$$

where we have substituted from (73). The ingredients for evaluating the summation (77) are given in the appendix. In particular it is shown that $C_k \sim 1$ and that

$$\alpha_k(t) \sim -2k^2\pi^2 t^2 + 2\pi i k\left(1 + t + t^2\right). \tag{78}$$

Therefore

$$\begin{aligned}\Phi(\xi) \sim \frac{1}{1-\tilde{\xi}} + \sum_k \Bigg\{ C_k \exp\Bigg[\theta\Bigg\{-\frac{2}{3}k^2\pi^2\left(\frac{\xi}{\theta^3}^3 - \frac{2}{\theta^3}^3\right) \\ +2\pi i k\left(\frac{\xi-2}{\theta} + \frac{\xi^2-2^2}{2\theta^2} + \frac{\xi^3-2^3}{3\theta^3}\right)\Bigg\}\Bigg] + c.c.\Bigg\}\end{aligned} \tag{79}$$

in the transition. This solution connects to (47) on the left and to (24) on the right.

8. Summary. In this brief section we collect together the asymptotic solution in the four layers which divide the interval. Starting at the right we have the following layers.

Boundary layer. From (75) we obtain

$$\phi(v) = \frac{1}{1-\gamma v/s}\left[1 - \frac{1-\gamma v/s}{1-\gamma/s}\exp\left[-\theta\int_{\gamma v/s}^{\gamma/s}\alpha_+(t)\,dt\right]\right]. \tag{80}$$

In our calculations we take

$$\alpha_+ \sim \alpha_+^0(t) + \alpha_+^1(t)/\theta; \tag{81}$$

α_+^0 is determined by (60) and α_+^1 by (61).

Intermediate layer. This is the integrate-and-fire region given by (24),

$$\phi(v) \sim \frac{1}{1-\gamma v/s}. \tag{82}$$

Transition layer. This follows from (79) and is given by

$$\begin{aligned}\phi(v) \sim \frac{1}{1-\gamma v/s} + \sum_k \exp\left[-\theta\left\{\frac{2}{3}k^2\pi^2\left[\left(\frac{\gamma v}{s}\right)^3 - \left(\frac{2}{\theta}\right)^3\right]\right\}\right] \\ - 2\pi i k\left(\left[\frac{\gamma v}{s} - \frac{2}{\theta}\right] + \frac{1}{2}\left[\left(\frac{\gamma v}{s}\right)^2 - \frac{2^2}{\theta^2}\right] + \frac{1}{3}\left[\left(\frac{\gamma v}{s}\right)^3 - \left(\frac{2}{\theta}\right)^3\right]\right) + c.c.\end{aligned} \tag{83}$$

Inner layer. This is covered by the exact treatment of section 4 and the subsequent asymptotic analysis of section 5.

In general,

$$\phi(v) = \Phi_n\left(\frac{v - nh}{h}\right) \text{ for } nh \le v \le (n+1)h \tag{84}$$

and, in particular,

$$\phi(v) = \delta(v/h) + \left(\frac{v}{h}\right)^{\theta-1}\phi^- \text{ for } 0 \le v < h \tag{85}$$

and

$$\phi(v) = \left(\frac{v}{h}\right)^{\theta-1}\phi^+ - \frac{\theta}{\theta-1}\left(\frac{v-h}{h}\right)^{\theta}\phi^- \text{ for } h < v \le 2h. \tag{86}$$

Recall that $\phi^- = \phi(h^-)$ and $\phi^+ = \phi^- - \theta$

It should be observed that (80) smoothly joins to (82) for fixed $v < 1$ as $\theta \uparrow \infty$, and similarly, that (83) smoothly joins (84) to (82). For computation, there is a choice of the integer ξ_*. If ξ_* is a small integer, then the inner layer solution (47) which contains $\xi_* + 1$ terms is relatively simple. However, by (66), the transition solution (83) essentially re-expresses the inner solution as a Fourier series (as (66) suggests); as the solution for ξ near small ξ_* departs from a sinusoid (see Figure 2), more terms in the sum (83) are required. Our computations use $\xi_* = 2$ for which at least five terms in the sum of (83) were used. The need for many terms arises from the nonsinusoidal character of the inner solution.

It remains for us to compute the firing rates. The firing rate follows from assembling all parts of the solution which we have just summarized and then applying (22). The result of these calculations are shown in Figure 3. As this figure indicates the diffusion approximation, without repairs, gives excellent results over the full range. This good agreement for firing rates can just as well be attributed to the integrate-and-fire density (24) which is responsible for a broad region of the density. The firing rate, (22), is quite insensitive to details of the density ρ. In dynamical situations this is no longer true and there are clear departures from the *exact* firing rate that is completed from solutions of (7) versus (28) [14].

It is of interest to observe that as a result of synaptic arrivals the solution for $s/\gamma < 1$ still has a nonzero firing rate. Examples of the equilibrium solution in this case are exhibited in Figure 5. The asymptotically small *toe* at $s/\gamma \approx .5$ shown in Figure 3 is due to this range.

9. The diffusion limit. The diffusion approximation introduced in section 3 was cast into doubt by the solution, (48), and and we now reconsider this limit. From (48) we see that for $v \approx 1, d^n\phi/dv^n = O\left[(1-\gamma/s)/h\right]^n$, and so from (49) the diffusion approximation breaks down unless γ/s is near enough to unity. When this is the case the diffusion approximation is valid in the neighborhood of $v = 1$. The WKB approximation, (54), implicitly assumes that $\alpha(t,\theta)$ is $O(1)$. But as (70) indicates α_0 diverges at $t = 1$, or equivalently when $v = s/\gamma$. Thus if $s/\gamma \approx 1$, the WKB approximation can be expected to fail. As s/γ passes across unity the diffusion approximation is valid and when this ratio is sufficiently large the WKB solution takes over. This is in Figure 2. For $s/\gamma = 1.2$, $\theta = 40$, the diffusion approximation better approximates the right-hand boundary while for $s/\gamma = 1.5$, $\theta = 50$, and beyond, the WKB is clearly the better approximation.

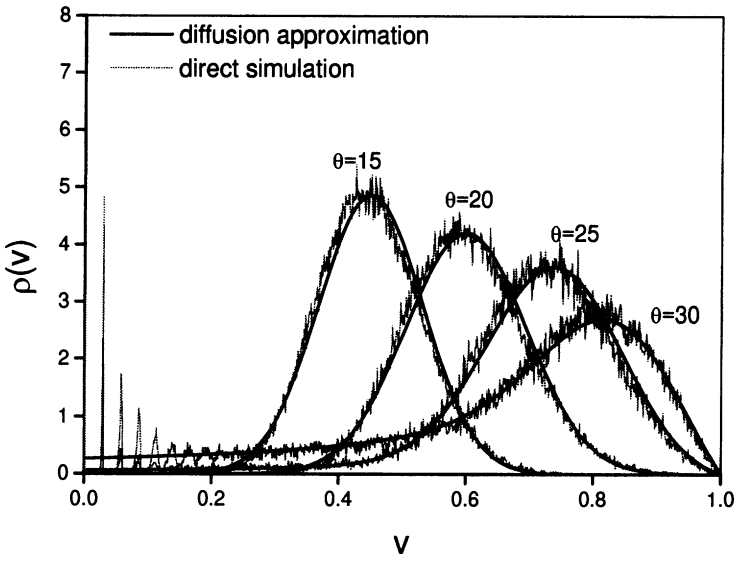

FIG. 4. *The position of the peak in the equilibrium probability density shifts toward the right as the external input is increased from $\theta = 15$ to $\theta = 30$. The gray jagged curves are the densities (for different values of θ) of a population of 10^4 leaky integrate-and-fire neurons computed by direct simulation* [14]. *The continuous curves which show the corresponding densities obtained in the diffusion limit agree well with the direct simulations. When the firing threshold is reached, neurons reentering the unit interval from the left generate the spiky appearance in the density near the left boundary.*

To consider the range $s \leq \gamma$ we rewrite (29) in the form

$$\phi = \frac{2}{h} e^{-\frac{\gamma}{sh}(v - s/\gamma)^2} \int_v^1 e^{\frac{\gamma}{sh}(v' - s/\gamma)^2} dv'. \tag{87}$$

The integrand peaks sharply at the endpoints. Although asymptotic evaluation of the integral is straightforward, some complexity results since one or both endpoints contribute depending on the values of γ/s and v. For example if $s \geq \gamma$, the left-hand endpoint furnishes the greater contribution and the result is given by (48). On the other hand if $s/\gamma < \frac{1}{2}$, the right-hand endpoint is the major contributor and in this case we obtain

$$\phi \sim \frac{e^{\theta(\gamma/s - 1)^2}}{1 - \gamma/s} e^{-\frac{\gamma}{sh}(v - s/\gamma)^2} \left(1 - e^{-2(\gamma/s)(1-v)/h}\right). \tag{88}$$

The shape yielded by this expression is dominated by a gaussian, centered at $v = s/\gamma$. A plot of this regime compared with direct simulation is shown in Figure 4.

Generally, the shape of ϕ, for $s/\gamma < 1$, is a gaussian centered at $v = s/\gamma$ and whose width is $\sqrt{sh/\gamma}$. It thus follows that $h\frac{d}{dv} = 0(\frac{1}{\sqrt{\theta}})$ and the Taylor expansion of the integral in (21) is a self-consistent approximation. Confirmation of this is found in Figure 4.

As pointed out earlier the diffusion limit is not valid for small values of v and therefore the boundary condition at $v = 0$, (11), is not met. Even when leakage exceeds current, $s/\gamma < 1$, this can clearly be repaired by connecting the diffusion solution, for small v, to the exact development and its asymptotics contained in

sections 4 and 5. Thus, when needed the transition analysis of section 8 can be used for $v < s/\gamma$ to connect the diffusion solution to the inner solution, as we did for $s/\gamma > 1$.

10. Concluding remarks. The description of a population of interacting neurons has been formulated in probabilistic terms to certain similarities with the Boltzmann equation of statistical mechanics [14]. While the description is nonlinear, the equilibrium case was reducible to a linear problem. In addition it was further shown that a single equilibrium solution corresponds to a range of cases starting with no neuronal connections to the possible interconnections discussed for (19). Due to the delay term in (7) the solution exhibits a high degree of complexity. As indicated in Figure 2 the analytically derived solution, as summarized in section 9, is in excellent agreement with the *exact* numerical equilibrium solution of (7). Figure 2 also contains the result of a direct simulation of as much as 90,000 interacting neurons acting under the same integrate-and-fire dynamics. The agreement is excellent. From the viewpoint of simulations it is noteworthy that integrating (7) is a modest calculation when compared with the direct simulation such as the one for 90,000 neurons.

The neuron model, defined by (4) and by the reset condition, was deliberately chosen to be near the minimal caricature able to still capture the three most essential dynamical features of a real impulse-encoding neuron. These are (1) the discounting of input from earlier times, which is achieved by the relaxation term $-\gamma v$; (2) a nonlinear thresholding mechanism for the fast voltage return of a charged cell membrane; and (3) a stochastic input jitter which arises from the temporal uncertainty of individual synaptic input events. The extreme simplification of the third feature, by the assumption of a single event size h, introduces what is probably the most unrealistic feature of this model, which is the extended sequence of narrow peaks in the probability density. We have also investigated a modified equation (4) in which the synaptic event size h is variable with a realistic probability distribution [14]. This new feature quickly spreads and damps the sequence of peaks. Although an *exact* solution is no longer available in this case, the same tactical asymptotic procedures used above still can be carried through to achieve an equilibrium solution. The generalization to include synaptic dynamics, inhibition, and interacting populations has also been considered [8], [14].

Appendix. The purpose of this appendix is to furnish background details for a number of calculations which have been left out of the body of the paper for a smoother reading.

Asymptotic integration. The integral which appears in (41) is a special case of

$$I(n', n; z) = \int_0^z \frac{(n'+s)^{\theta-1}}{(n+s)^{\theta}} ds;\ n > n'. \tag{A1}$$

This more general form is needed in arriving at (47). We observe that for $p >> 1$ the main contribution to the integral comes from the neighborhood of the upper endpoint. We therefore set $s = z - u$ and rewrite (A1) as

$$I = \int_0^z \frac{du}{n+z-u} \exp\left[pE(n', n, z, u)\right], \tag{A2}$$

where

$$E = \ln(n'+z-u) - \ln(n+z-u). \tag{A3}$$

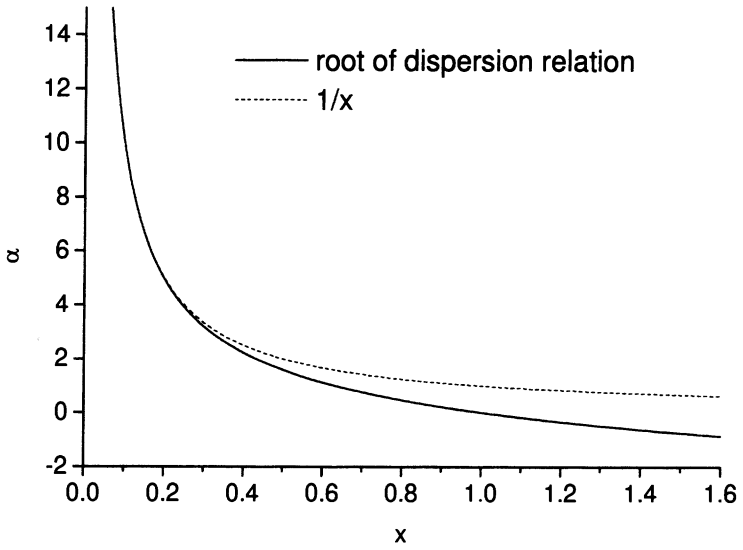

FIG. 5. *The positive root of the dispersion relation,* (A6), *is shown by the solid curve. Near* $x = 0$ *it is well approximated by the function* $(1/x)$, *plotted as a dashed curve.*

For z bounded away from the origin we may apply Watson's lemma or equivalently expand E in the neighborhood of $u = 0$:

$$E = \ln\left(\frac{n'+z}{n+z}\right) - \frac{u}{n'+z} + \frac{u}{n+z} + O\left(\frac{u^2}{(n+z)^2}\right). \tag{A4}$$

If (A4) is substituted into (A2) we obtain

$$I \sim \frac{(n'+z)^{\theta}}{(n+z)^{\theta-1}(n-n')^{\theta-1}}. \tag{A5}$$

The error term which appears in (A4) indicates that $n^2 << \theta$ is a sufficient condition for the asymptotics. To see this observe that (A4) substituted into (A3) shows that only the neighborhood of the origin $u \sim n/p$ contributes to the integral.

Roots of the dispersion relation (Figure 5*).* The dispersion relation

$$x\alpha = 1 - e^{-\alpha}\ ;\ x \geq 0 \tag{A6}$$

figures in the calculation in two ways, in the WKB solution (60), and in (65) which is the solution of (62).

An exact solution to (A6) is

$$\alpha_0 = 0. \tag{A7}$$

There is one more real solution which is positive for $x \leq 1$, and we denote it by α_+. In fact for $0 < x << 1$ we see from (A6) that

$$\alpha_+ \sim \frac{1}{x}. \tag{A8}$$

A graph of the root and comparison with (A8) is shown in the figure.

There are infinitely many roots of (A6) in the left half of the complex α-plane and a perturbative analysis for small x yields

$$\alpha_k = -2k^2\pi^2x^2 + 2\pi ki\left(1 + x + x^2\right) + 0\left(x^3\right). \tag{A9}$$

The function $\Phi(\sigma)$. It was found that the full WKB solution depends functionally on the integral

$$\Phi(\sigma) = \int_0^1 e^{-\sigma\tau}\Phi_{k-1}(\tau)\,d\tau. \tag{A10}$$

Instead of evaluating this in general we take $k = 2$, which is the case used in our calculations. In this case we can substitute (46) in (A10) to obtain

$$\Phi(\sigma) \sim \int_0^1 e^{-\sigma\tau}\left\{\left(\frac{1+\tau}{2}\right)^{\theta-1}\Phi_2^0 + \left[\left(\frac{1+\tau}{2}\right)^{\theta-1} - \tau^{p+1}\right]\frac{\theta}{\theta-1}\phi^-\right\}d\tau. \tag{A11}$$

The support of the curly bracket lies in the neighborhood of $\tau = 1$. If we write $\tau = 1 - u$, then

$$\Phi(\sigma) = e^{-\sigma}\int_0^1 e^{\sigma u}\left\{\left(1 - \frac{u}{2}\right)^{\theta-1}\Phi_2^0 + \left[\left(1 - \frac{u}{2}\right)^{\theta-1} - (1-u)^{\theta}\right]\frac{\theta}{\theta-1}\phi^-\right\}du. \tag{A12}$$

Next if we take $\left(1 - \frac{u}{2}\right)^p \sim e^{-pu/2}$ and $(1-u)^p \sim e^{-pu}$, we obtain

$$\Phi(\sigma) \sim -e^{-\sigma}\left\{\frac{1 - e^{\sigma-(\theta-1)/2}}{\sigma - (\theta-1)/2}\Phi_2^0 + \frac{\theta}{\theta-1}\phi^-\left[\frac{1 - e^{\sigma-(\theta-)1/2}}{\sigma-(\theta-1)/2} - \frac{1-e^{\sigma-\theta}}{\sigma-\theta}\right]\right\}. \tag{A13}$$

We observe that each quotient is nonsingular where its denominator vanishes, in agreement with (A11) which has no singularities in the finite plane.

In the solution of either (52) or (62) we require the evaluation of $\Phi(\sigma)$ at the roots of the dispersion relation (65), and from that follows the evaluation of the coefficients C_+, C_0, and C_k. As seen from (42) $\phi^- \approx \theta$, which is therefore relatively large. On the other hand, as will be seen momentarily, Φ_2^0 is exponentially small, for $\theta \approx 40$, $\Phi_2^0 = 0\left(10^{-7}\right)$. If these two observations are applied to (A13) we obtain

$$\Phi(\sigma) \sim -e^{-\sigma}\frac{\theta^2}{\theta-1}\left[\frac{1 - e^{\sigma-(\theta-1)/2}}{\sigma-(\theta-1)/2} - \frac{1-e^{\sigma-\theta}}{\sigma-\theta}\right]. \tag{A14}$$

Thus

$$\Phi(\sigma = 0) \sim -1 \tag{A15}$$

and therefore from (67)

$$C_0 \sim \frac{1}{1-\xi_*}. \tag{A16}$$

Next, since $\widetilde{\xi}_* = 2/\theta$, it follows that $\sigma_+ \sim p/2$ from which it follows that

$$C_+ \sim \left(\Phi_2^0 \widetilde{\xi}_* - \frac{\theta^2 e^{-\theta/2}}{\theta - 1} \right) / \widetilde{\xi}_*. \tag{A17}$$

For the remaining roots

$$\varphi(\sigma_k) = \varphi_k \sim e^{-\sigma_k} \tag{A18}$$

and

$$C_k \sim 1. \tag{A19}$$

REFERENCES

[1] L. ABBOTT AND C. VAN VREESWIJK, *Asynchronous states in networks of pulse-coupled oscillators*, Phys. Rev. E, 48 (1993), pp. 1483–1490.

[2] M. ABELES, *Corticonics: Neural Circuits of the Cerebral Cortex*, Cambridge University Press, Cambridge, UK, 1991.

[3] T. CHAWANYA, T. AOYAGI, I. NISHIKAWA, K. OKUDA, AND Y. KURAMOTO, *A model for feature linking via collective oscillations in the primary visual cortex*, Biological Cybernetics, 68 (1993), pp. 483–490.

[4] M.-N. CHEE-ORTS, K. PURPURA, AND L. OPTICAN, *A Dynamical Model of the Primate's Early Visual Pathway: Effect of Luminance Contrast, Spatial Scale, and Spatial Orientation in Shaping Neuronal Firing Patterns*, unpublished report, 1996.

[5] W. GERSTNER, *Time structure of the activity in neural network models*, Phys. Rev. E, 51 (1995), pp. 738–758.

[6] P. JOHANNESMA, *Stochastic Neural Activity: A Theoretical Investigation*, Ph.D. thesis, University of Nijmegen, Nijmegen, The Netherlands, 1969.

[7] B. KNIGHT, *Dynamics of encoding in a population of neurons*, J. Gen. Physiol., 59 (1972a), pp. 734–766.

[8] B. KNIGHT, *Dynamics of encoding in neuron populations: Some general mathematical features*, Neural Computation, 12 (2000), pp. 473–518.

[9] B. KNIGHT, D. MANIN, AND L. SIROVICH, *Dynamical models of interacting neuron populations*, in Symposium on Robotics and Cybernetics: Computational Engineering in Systems Applications, E.C. Gerf, ed., Cite Scientifique, Lille, France, 1996.

[10] C. KOCH AND I. SEGEV, *Methods in Neuronal Modeling: from Synapses to Networks*, MIT Press, Cambridge, MA, 1989.

[11] M. MACKEY AND L. GLASS, *Oscillation and chaos in physiological control systems*, Science, 197 (1977), pp. 287–289.

[12] T. MCKENNA, J. DAVIS, AND S. ZORNETZER, *Single Neuron Computation*, Academic Press, San Diego, CA, 1992.

[13] E. MIROLLO AND S. STROGATZ, *Synchronization of pulse-coupled biological oscillators*, SIAM J. Appl. Math., 50 (1990), pp. 1645–1662.

[14] A. OMURTAG, B. KNIGHT, AND L. SIROVICH, *On the simulation of large populations of neurons*, J. Comp. Neurosci., 8 (2000), pp. 51–63.

[15] C. PESKIN, *Mathematical Aspects of Heart Physiology*, Lecture Notes, Courant Institute of Mathematical Sciences, New York University, New York, 1975.

[16] L. SIROVICH, B. KNIGHT, AND A. OMURTAG, *Dynamics of Neuronal Populations: The Stability of Equilibria*, submitted.

[17] D. SOMERS, S. NELSON, AND M. SUR, *An emergent model of orientation selectivity in cat visual cortex simple cells*, J. Neurosci., 15 (1995), pp. 5448–5465.

[18] R. STEIN, *A theoretical analysis of neuronal variability*, Biophys. J., 5 (1965), pp. 173–194.

[19] H. C. TUCKWELL, *Introduction to Theoretical Neurobiology*, Vol. 2, Cambridge University Press, Cambridge, UK, 1988.

[20] C. VAN VREESWIJK AND L. ABBOTT, *Self-sustained firing in populations of integrate-and-fire neurons*, SIAM J. Appl. Math., 53 (1993), pp. 253–264.

[21] W. WILBUR AND J. RINZEL, *An analysis of Stein's model for stochastic neuronal excitation*, Biological Cybernetics, 45 (1982), pp. 107–114.

[22] F. WORGOTTER AND C. KOCH, *A detailed model of the primary visual pathway in the cat: Comparision of afferent excitatory and intracortical inhibitory connection schemes for orientation selectivity*, J. Neurosci., 11 (1991), pp. 1959–1979.